We are IntechOpen,
the world's leading publisher of
Open Access books
Built by scientists, for scientists

4,800
Open access books available

122,000
International authors and editors

135M
Downloads

Our authors are among the

154
Countries delivered to

TOP 1%
most cited scientists

12.2%
Contributors from top 500 universities

CLARIVATE ANALYTICS

BOOK CITATION INDEX

INDEXED

WEB OF SCIENCE™

Selection of our books indexed in the Book Citation Index
in Web of Science™ Core Collection (BKCI)

Interested in publishing with us?
Contact book.department@intechopen.com

Numbers displayed above are based on latest data collected.
For more information visit www.intechopen.com

Transverse Vibration Control for Cable Stayed Bridge Under Construction Using Active Mass Damper

Hao Chen, Zhi Sun and Limin Sun

Additional information is available at the end of the chapter

1. Introduction

Since the erection of the Stromaund Bridge of Sweden in 1956, cable-stayed bridge, as an efficient and economic bridge type to surmount a long-distance obstacle, has attracted more and more interests both from bridge engineering community and from the society and government. Nowadays, the cable stayed bridge is the most competitive type for the bridge with the span of 300-1000 meters. For a cable supported bridge, which is generally quite flexible and of low damping, its vibration under ambient excitation (such as the wind and ground motion excitation) and operational loading (such as the vehicle and train loads) is quite critical for its safety, serviceability and durability. Vibration control countermeasures, such as the installation of the energy dissipating devices, are thus required [1, 2]. Structural active control, which applies a counter-force induced by a control device to mitigate structural vibration, has been widely proposed for the vibration control of cable stayed bridges and proven to be efficient by many researchers [3-6].

Although the vibration response of a fully erected cable-stayed bridge should be controlled, a cable-stayed bridge under construction, which is of low damping and not as stable as the completed structure, is generally more vulnerable to dynamic loadings. During the construction stage, the cable pylons were generally erected firstly and the cable and main girders are then hang on the pylons symmetrically in a double-cantilever way. With the increase of the cantilever length, the bridge is more and more flexible. When the girder is on its longest double-cantilever state, the bridge is the most vulnerable to the external disturbance (such as the ambient wind fluctuation and ground motions). Moreover, if the cables, pylons and main girder of the bridge are all steel components and thus the damping of the bridge is very low, its vibration under ambient excitations will be quite large. The vibration reduction countermeasures are thus in great demand. Frederic

conducted several mock-up tests representing a cable-stayed bridge during the construction stage [7]. Since the control objective was set to reduce the girder vertical vibration response or cable parametric vibration response, the active tendon was installed as the control device. While for a cable stayed bridge under uncontrollable ambient excitations, structure will vibrate not only in the vertical direction but also in the transverse direction. Moreover, since the bridges are generally designed to carry the vertical loads, the unexpected transverse loads, especially the transverse dynamic loads, will induce structural safety and durability problems. It is thus of crucial importance to install some vibration reduction devices to control bridge transverse vibration. For this type of structure vibration control problem, the active mass damper (AMD) or the active tuned mass damper (ATMD) will be a competent candidate [8, 9].

In this chapter, the general procedure and key issues on adopting an active control device, the active mass damper (AMD), for vibration control of cable stayed bridges under construction are presented. Taking a typical cable stayed bridge as the prototype structure; a lab-scale test structure was designed and fabricated firstly. A baseline FEM model was then setup and updated according to the modal frequencies measured from structural vibration test. A numerical study to simulate the bridge-AMD control system was conducted and an efficient LQG-based controller is designed. Based on that, an experimental implementation of AMD control of the transverse vibration of the bridge model was performed.

2. Model structure description and vibration test

The lab-scale bridge model studied in this chapter is designed according to a prototype cable-stayed bridge, the Third Nanjing Yangtze River Bridge located in Jiangsu Province of China. Since the prototype bridge is of all the characteristics of a modern cable-stayed bridge, the test model is assumed to be a good test bed to study the feasibility of active structural control applied to cable-stayed bridges under construction. The test model was designed and fabricated to simulate the longest double cantilever state during the construction stage of the prototype bridge. Since structural dynamic response control is the main focus of this chapter, the test model is preliminarily designed according to the dynamic scaling laws. However, concerning the restriction of test conditions, some modifications were made during the detailed design of the model bridge [10]. Fig. 1 shows the dimension of the designed model bridge. The bridge is composed of a 1.433 meters high cable pylon, a 3.08 meters long main girder, and six couples of stay cables. The cross section of the main girder is a rectangular of 16 mm wide and 10 mm high. At two ends of the main girder, the 3.6 kg and 3.8 kg weight AMD orbits were installed on the side span and main span respectively. The stay cables are made of steel wire with the diameter of 1 mm. At the upper end of each cable, an original 30 cm long spring was installed and adjusted to simulate the cable force. The cable forces were adjusted to provide supporting force to the main girder and to force it to match the designed layout of the test bridge. Table 1 shows the length, Young's Modulus and computed cable force for the cables. All of the components were made of steel. Since the model consists of only one cable pylon and no other piers, it is symmetric with respect to the cable pylon.
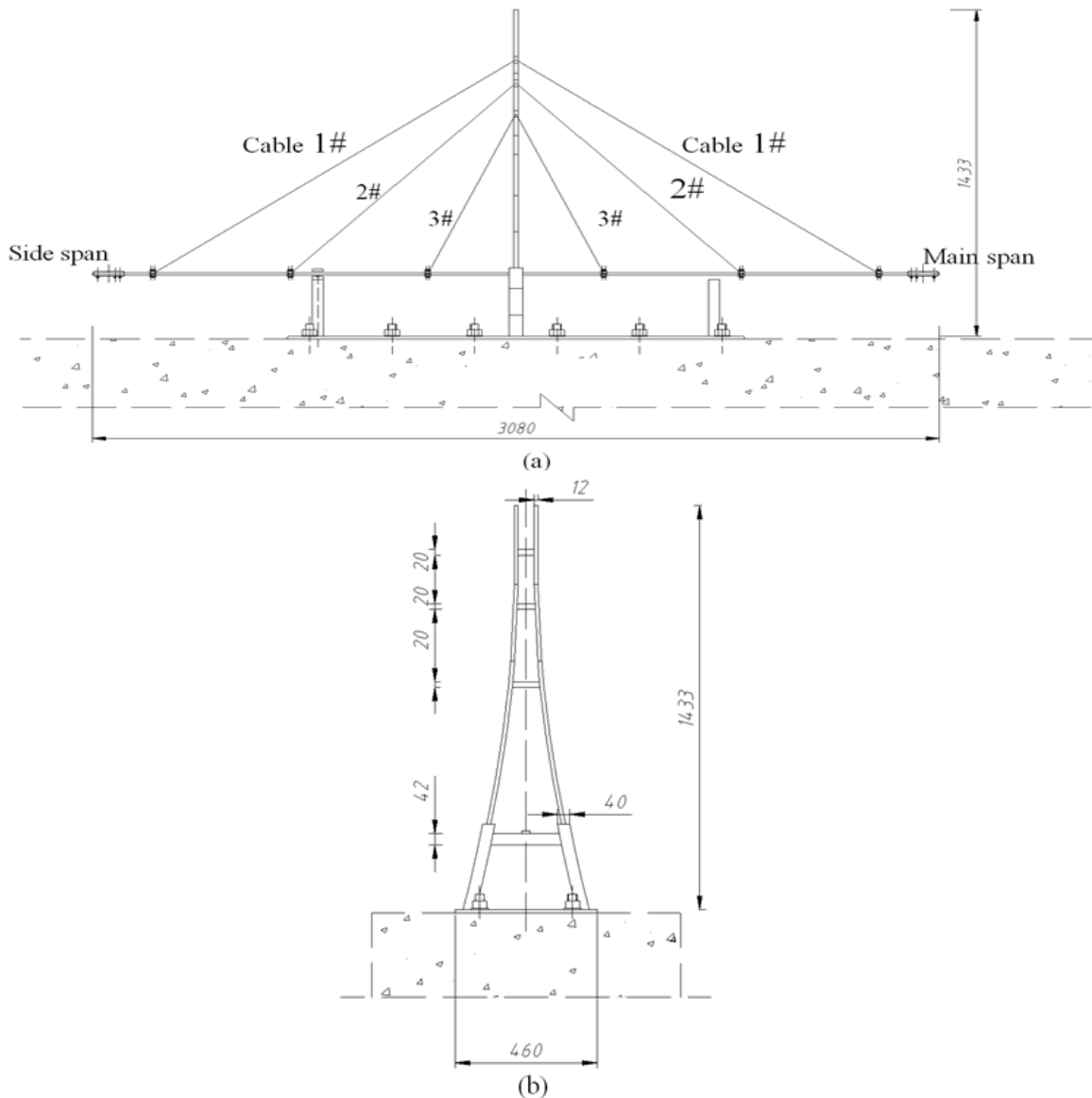
**Figure 1.** The elevation view (a) and side view (b) of the test model (unit: mm)

Cable No.	1#	2#	3#
Young's Modulus (Mpa)	451.7	327.0	216.0
Length with spring (m)	1.62	1.17	0.77
Spring Force (N)	32.0	13.9	7.2

Table 1. Cable parameters

Num.	1	2	3	4	5	6	7	8
Sensitivity (mv/g)	134.6	140.8	127.4	134.6	149.2	138.3	138.5	130.8
Location (m)	0.06	0.32	0.62	1.02	2.06	2.46	2.76	3.02

Table 2. Sensor sensitivity and location distances from the tip end of the side span

Vibration tests under forced excitations were conducted to identify the dynamic characteristics of the bridge model. Eight accelerometers (as described in Table 2) were distributed along the main girder both on the side span and the main span to collect structural acceleration responses at a sampling frequency of 50 Hz (as shown in Fig. 2a). A transverse impulse force was acted on the cantilever end of the side span to excite the structure. Concerning that the bridge model is symmetrical about the cable pylon and thus of repeated or close frequency modes, a modal identification algorithm of the capacity to identify the close modes, the wavelet based modal identification method developed by the research group, is used [11]. During the analysis, the mother wavelet function adopted is the complex Morlet function with the central frequency of 300 Hz and the scale increment is set to be 0.25 during the analysis. Fig. 2b shows the wavelet scalgram of a set of response measurement on the tip end of the side span. As shown in the figure, structural transverse vibration responses were dominated by two modes at the scale of 168.0 and 176.5, which correspond to the vibration modes of the natural frequencies of 1.701 Hz and 1.786 Hz, respectively. This figure also shows that the adopted modal identification method can separate these two close modes successfully. Structural modal parameters can then be estimated and the results are shown in Table 3.
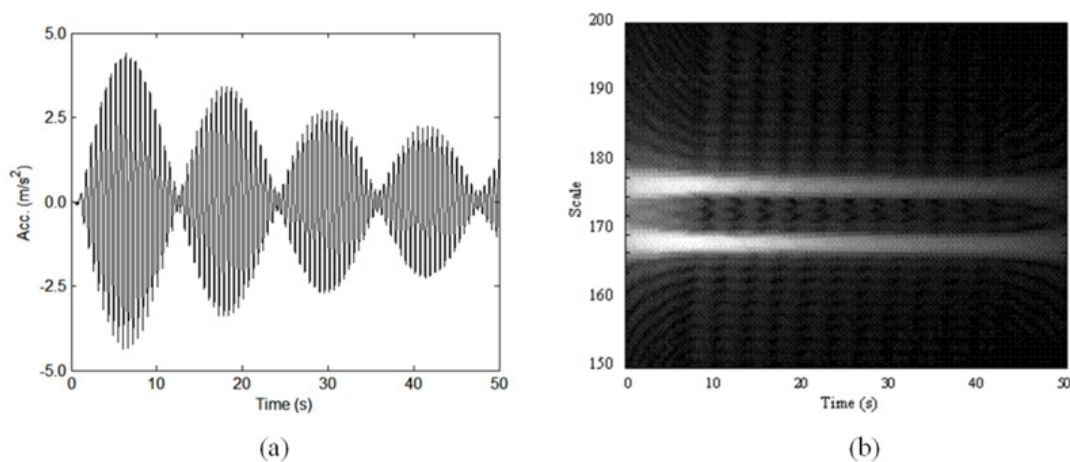
Figure 2. Collected (a) free decay acceleration response and (b) its wavelet scalogram

3. Numerical modeling and model updating

For structural active control, a baseline numerical model is generally required for controller design. A FEM bridge model is thus setup in ANSYS according to the design diagram of the bridge model. The cable is modeled using a 3D uniaxial tension-only truss element. Equivalent modulus for the cables without spring are computed using Ernst formula and then series wound equivalent modulus for the cable with spring can be established. Other structural elements are all modeled using 3D elastic beam element. Cables are connected to the main girder using rigid beam element. Additional masses were modeled using isotropic mass element. The cable pylons and the main girder are linked by coupling the horizontal projective intersection points of the lowest transverse beam of the pylon with the main girder. The six DOFs at the feet of the pylon are fixed.

		The first transverse symmetrical bending (TSB) mode	The first transverse anti-symmetrical bending (TAB) mode
Frequency	Test	1.701 Hz	1.786 Hz
	Initial Model	1.848 Hz	1.856 Hz
	Updated Model	1.787 Hz	1.786 Hz
Mode Shape	Test	[1.00 0.86 0.70 0.32 0.00 0.30 0.70 0.90 0.99]	[1.00 0.84 0.72 0.28 0.00 -0.32 -0.70 -0.86 -0.99]
	Initial Model	[1.00 0.74 0.46 0.17 0.00 0.13 0.38 0.60 0.81]	[1.00 0.74 0.47 0.17 0.00 -0.14 -0.38 -0.60 -0.81]
	Updated Model	[1.00 0.74 0.46 0.17 0.00 0.17 0.46 0.74 1.00	[1.00 0.74 0.46 0.17 0.00 -0.17 -0.46 -0.74 -1.00]
MAC*	Initial Model	0.9620	0.9620
	Updated Model	0.9722	0.9718

* MAC (modal assurance criteria) is defined to be a correlation coefficient of two mode shape vectors.

Table 3. The computed modal parameters before and after model updating compared with the tested mode parameters

Taken eigenvalue analysis of the numerical model, structural natural frequencies and mode shape vectors can be computed. Table 4 shows the computed modal parameters of the transverse bending modes. As shown in the table, since the sum of the effective mass of the first transverse anti-symmetric bending mode (TAB) and the first transverse symmetric bending mode (TSB) is 80.1% of the sum of the effective mass of all transverse modes, these 2 transversal modes dominant the transverse vibration of the bridge. Fig. 3 shows the mode shape of these two transverse bending modes.

No.	Frequency (Hz)	Mode description	Effective mass (kg)
1	1.848	The first TAB mode	6.00
2	1.856	The first TSB mode	6.00
3	19.802	The second TAB mode	0.94
4	19.848	The second TSB mode	0.94

Table 4. The computed natural frequencies for the first 4 transverse modes of the main girder

Comparing the natural frequencies obtained from the eigenvalue analysis on the numerical model and the vibration test on the test bridge, some differences can be observed (as shown in Table 3). A model updating process is thus conducted to get an accurate baseline numerical model. The results of the sensitivity analysis show that the vertical and transverse vibration modes are sensitive to the tip mass magnitude, while the Young's module of the cable is critical for vertical bending modes. So these two parameters were updated: the tip masses of two spans were updated from 3.8kg and 3.6kg to 4.16kg, respectively, and the spring modulus was updated from 220N/m to 203N/m. Table 4 shows the natural frequencies and mode shapes of the updated model. As shown, the modal parameters of the first TSB and TAB modes have a good match with the modal test results.
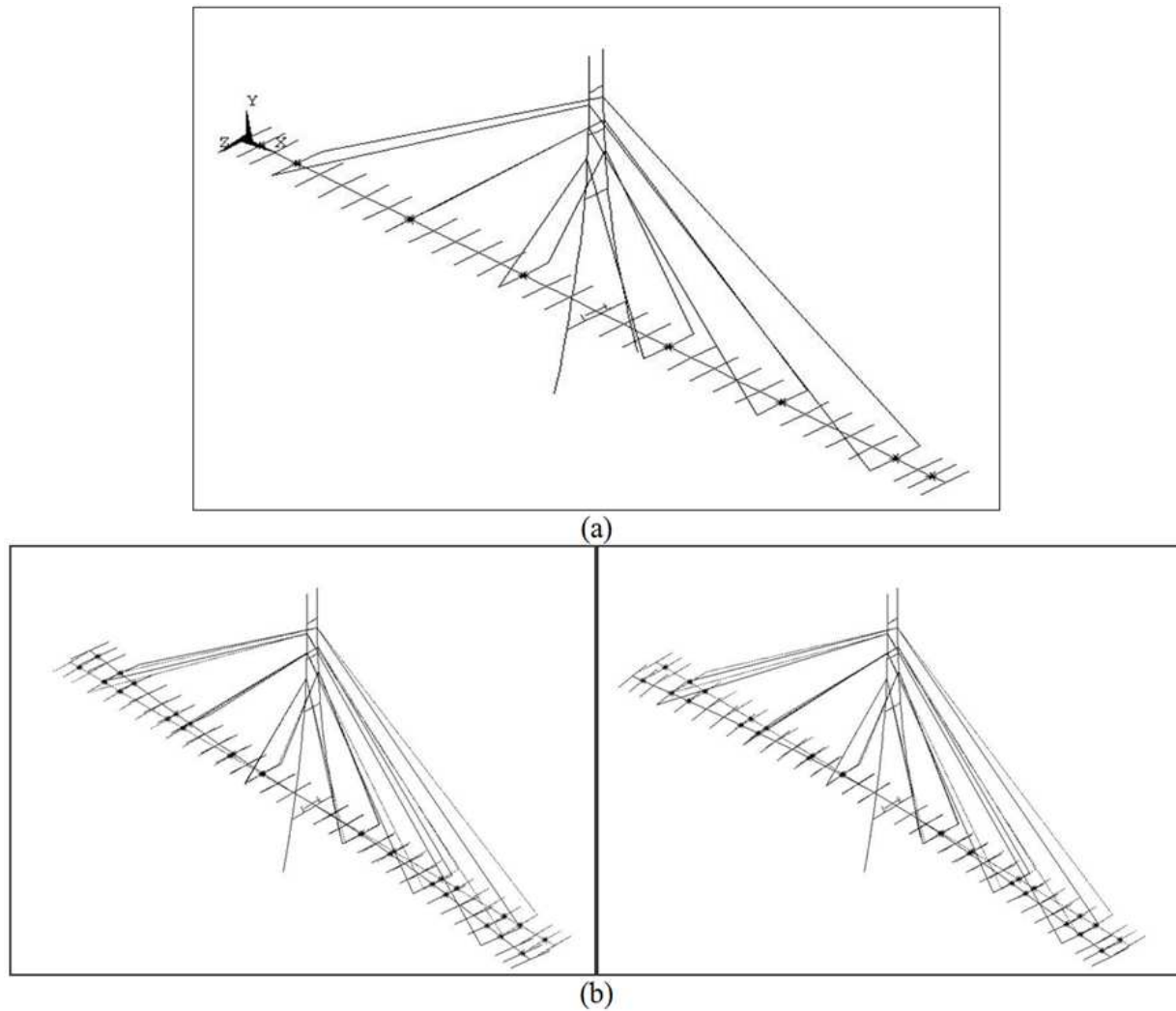
Figure 3. The baseline FEM model (a) setup in ANSYS and the computed mode shape (b) of the first transverse anti-symmetric and symmetric bending mode

4. Control system simulation

Based on the baseline numerical model updated according to dynamic measured structural modal parameters, a system simulation study is conducted. For a bridge-AMD system, its governing equation of motion is

$$M_s\ddot{X}(t) + C_s\dot{X}(t) + K_sX(t) = F_e(t) + D^TT^Tf_d(t) \tag{1}$$

$$m_d\ddot{x}_d(t) + f_d(t) = 0 \tag{2}$$

$$f_d(t) = -c_d[\dot{x}_d(t) - TD\dot{X}] + b_du(t) \tag{3}$$

where, M_s, C_s, and K_s are the mass, damping and stiffness matrices of the bridge structure; $X(t) = \begin{bmatrix} x_1 \cdots x_i \cdots x_n \end{bmatrix}'$ is a n-dimensional vector, in which x_i is the displacement response vector of the ith DOF of the structure and n is the number of the DOF of the structure; $F_e(t)$

is the excitation force vector acting on the structure; $D = \begin{bmatrix} 0 & I & 0 \end{bmatrix}$ is the AMD location matrix, in which 0 and I are zero and identity matrix with appropriate sizes; $f_d(t)$ is the actuation force on the structure applied by the AMD ; T is the transfer matrix from the affiliated nodes of AMD to the principle nodes of the structure ; $m_d = diag\begin{bmatrix} m_{d1} \cdots m_{di} \cdots m_{dl} \end{bmatrix}$ is the mass matrix of the AMDs, in which m_{di} is the mass of the ith AMD; $x_d(t)$ are absolute displacement of the AMD to the bridge structure, respectively; c_d is the viscous coefficient of the AMD; b_d is the force-voltage coefficient of the AMD and $u(t)$ is the control input voltage.

Since the numerical model of a complex structure is generally of a large amount of DOFs, for example in this study the FEM model obtained from the last section is of 1188 DOFs, this will induce great computation difficulty to design the controller according to this so called full order model. A reduced order model is thus required. In this study, the critical modal reduction method is adopted for this purpose because this method can greatly reduce structural DOFs and the reduced order model is of clear physical meaning [12, 13]. Concerning a structure whose vibration is dominated by the first r modes, its dynamic response can be approximately expressed as $X(t) \cong \sum_{i=1}^{r} \phi_i Y_i(t)$ and the full order model can thus be reduced to an r-order reduced order model. The governing equation of motion for this reduced order model is

$$\hat{M}_s \ddot{Y}(t) + (\hat{C}_s - c_d \phi^T D^T T^T T D \phi) \dot{Y}(t) + \hat{K}_s Y(t) + \phi^T D^T T^T c_d \dot{x}_d(t) = \hat{F}_e(t) + \phi^T D^T T^T b_d u(t) \quad (4)$$

$$m_d \ddot{x}_d(t) - c_d \dot{x}_d(t) + c_d T D \phi \dot{Y} = -b_d u(t) \quad (5)$$

where, $Y(t)$ is the modal response vector superposed by the modal responses of the rth principle modes; ϕ is the generalized mode shape matrix composed of the mode shape vectors of the first r principle modes; $\hat{M}_s = \phi^T M_s \phi$, $\hat{C}_s = \phi^T C_s \phi$ and $\hat{K}_s = \phi^T K_s \phi$ are structural generalized mass, damping and stiffness matrices, respectively; $\hat{F}_e = \phi^T F_e$ is the generalized excitation vectors. In this study, since the vibration responses of the first two transversal vibration modes are the most accountable for structural transverse vibration, structural modal mass, stiffness and damping matrices are computed using the modal parameters of these two modes. Correspondingly, the governing equation of motion for the reduced order bridge-AMD system can be derived.

For this reduced order bridge-AMD system, its state space equation is

$$\dot{x}_r = A_r x_r + B_r u + E_r w \quad (6)$$

$$z_r = C_r^z x_r + D_r^z u + E_r^z w \quad (7)$$

$$y_r = C_r^y x_r + D_r^y u + E_r^y w \quad (8)$$

where, x_r is an a dimensional state-space vector, $a = 2r + l$, r and l are the number of DOF for the reduced order structure and the number of the installed AMD, respectively; A_r is an $a{\times}a$ system matrix; u is the control input vector for the l AMDs; B_r is an $a{\times}l$ AMD location matrix; w is the generalized modal excitation vector; E_r is an $a{\times}r$ excitation matrix; z_r is an l dimensional control output vector; y_r is a q dimensional observer output vector. The system matrices can be expressed as:

$$x = \left\{ \begin{array}{c} Y \\ \dot{Y} \\ \dot{x}_d \end{array} \right\}; \; A_r = \begin{bmatrix} 0 & I & 0 \\ -\hat{M}_s^{-1}\hat{K}_s & -\hat{M}_s^{-1}\hat{C}^* & -\hat{M}_s^{-1}\phi^T D^T T^T c_d \\ 0 & m_d^{-1}c_d H & m_d^{-1}c_d \end{bmatrix}; \; B_r = \begin{bmatrix} 0 \\ \hat{M}_s^{-1}\hat{H}b_d \\ -m_d^{-1}b_d \end{bmatrix}; \; E_r = \begin{bmatrix} 0 \\ \hat{M}_s^{-1} \\ 0 \end{bmatrix};$$

$$C_r^z = \alpha \begin{bmatrix} I \\ \begin{bmatrix} 0 & I \end{bmatrix} A_r \end{bmatrix}; \; D_r^z = \alpha \begin{bmatrix} I \\ \begin{bmatrix} 0 & I \end{bmatrix} B_r \end{bmatrix}; \; E_r^z = \alpha \begin{bmatrix} 0 \\ \begin{bmatrix} 0 & I \end{bmatrix} E_r \end{bmatrix};$$

$$C_r^y = \beta \begin{bmatrix} I \\ \begin{bmatrix} 0 & I \end{bmatrix} A_r \end{bmatrix}; \; D_r^y = \beta \begin{bmatrix} I \\ \begin{bmatrix} 0 & I \end{bmatrix} B_r \end{bmatrix}; \; E_r^y = \beta \begin{bmatrix} 0 \\ \begin{bmatrix} 0 & I \end{bmatrix} E_r \end{bmatrix};$$

where $\hat{C}^* = \hat{C}_S - \hat{H}c_d\hat{H}^T$; $\hat{H} = \begin{bmatrix} -TD\phi & I \end{bmatrix}^T$; 0 and I are zero and identity matrix with appropriate sizes; α and β are appropriately selected weighting matrix to adjust the optimize objective of the controller, respectively. The control output vector z_r and the observer output vector y_r are the displacement, velocity and acceleration responses of the bridge structure or the AMDs.

The control output and observer output matrices C_r^z, D_r^z, C_r^y, and D_r^y are determined according to the sensor and actuator placement. The sensor placement should basically satisfy the following observability criteria $rank \begin{bmatrix} A_r - \lambda I \\ C_r^y \end{bmatrix} = a$, where λ is an arbitrary complex number [14]. For a system with n modes of repeated or close frequency, n sensors are required for full state response measurement. In this study, to provide redundant channels to collect structural response, eight accelerometers, the same as aforementioned in the modal test, are installed along the main girder during the control process. The actuators are placed on the girder by checking the following controllability criteria $a = rank \begin{bmatrix} A_r - \lambda I, B_r \end{bmatrix}$. In this study, different schemes for AMD placement will be discussed in detail in the following sections.

5. Controller design

The design of a controller is very important for the success of structural active vibration control. In this study, the LQG control algorithm is adopted since this control algorithm can offer excellent control performance and is of good robustness as shown in some preliminary

study [10]. During the controller design process, the excitation is assumed to be a stationary white noise, and the following cost function is set as the control objective:

$$J = \lim_{t \to \infty} E\left[\int_0^t (z_r{}^T Q z_r + u^T R u) dt \right] \tag{9}$$

where z_r, system output variables, are set to be the transverse displacement or acceleration response at the tip ends; Q, a square matrix of the same order as z_r, equals to the multiplication of an identity matrix with a parameter q; u is a control force variable; R, the active force weight matrix, is set to be an identity matrix of the same order as the number of AMD applied. The design of the LQG controller is to adjust the weight parameter q via optimizing the performance of the system with compensator under the limitation of energy supply. The design of the controller relies on the full state feedback vector X_r. Since limited sensors are mounted on the structure, this full state vector cannot be directly measured but be estimated from the sensor measurements. When the excitation forces w and the measurement noise v are uncorrelated white noise process, the Kalman-Bucy filter is employed to get an estimation of the state vector X_r [15].

To obtain a good controller for experimental implementation, a series of numerical analysis with different value of weight parameter q are conducted. During the numerical analysis, structural modal damping coefficients are set to be the same as the real measured modal damping ratios. A scaled *El Centro* earthquake time history, whose dominant frequency band covers the first 2 transverse modal frequencies of the bridge, is adopted to excite the bridge in the numerical study. Two AMD placement strategies are employed for the comparison of optimal actuator location. These two strategies are the strategy of one AMD placed at the tip end of the main span (named S1) and the strategy of two AMDs placed at the tip ends of both spans (named S2). The AMDs are simulated to be the two electric servo-type AMD carts provided by Quanser Inc. with the following expression of the actuation force

$$f_d^1(t) = 8.246\dot{x}_d(t) + 1.42u(t) \tag{10}$$

$$f_d^2(t) = 12.576\dot{x}_d(t) + 1.73u(t) \tag{11}$$

To simulate a more practical control condition during experimental implementation, the following constraint condition is adopted: 1) The discrete digital computation is employed for the controller computation with the sampling frequency of 500Hz; 2) The precision of the A/D converter is set to be 12-bits and the range of the input voltage is set to be ± 5 V; 3) The measurement noise of a root mean square (RMS) value of 0.015 V is added into each channel of the acceleration responses, which corresponds to the 0.3% of voltage range of the A/D converter; 4) The maximum actuation voltage is set to be ± 5 V with the corresponding RMS voltage of 1.67 V and the maximum actuation displacement is set to be ± 0.08 m with the corresponding RMS displacement of 0.027 m.
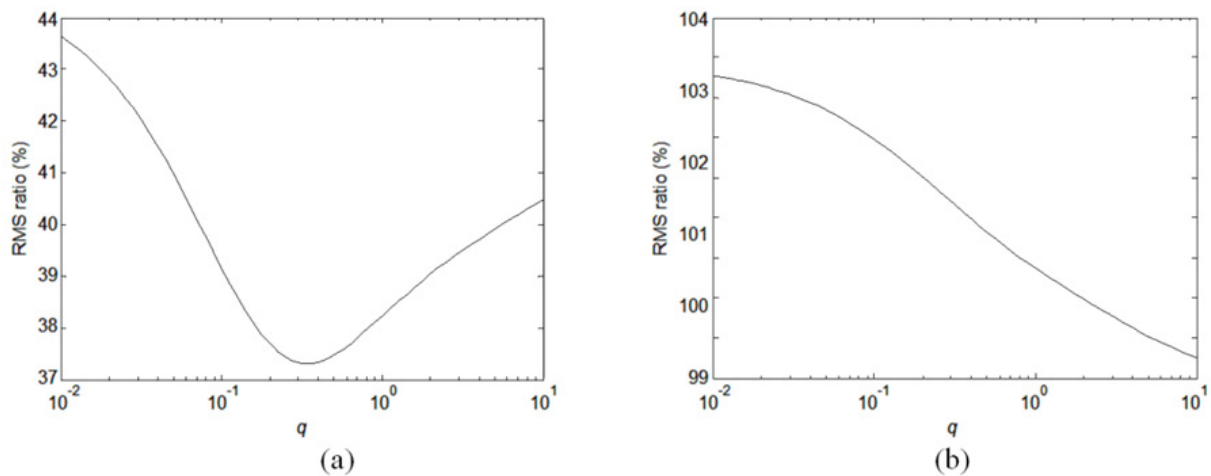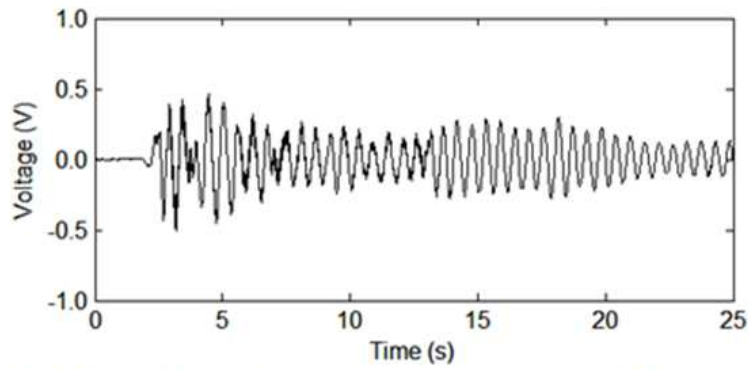
Figure 4. The ratio of the controlled acceleration RMS value to uncontrolled RMS value at the tip ends of the side span (a) and main span (b) with respect to the weighting parameter q for S1 control

For S1 control, a series of numerical studies simulating the control system with one AMD cart installed on the tip end of the main span of the bridge, whose actuation force is expressed as Eq. (10), are conducted when the weighting parameter q varies from 0.01 to 10. Fig. 4 shows the relative RMS ratio of the controlled acceleration response to the uncontrolled acceleration response at the tip end of both main span and side span with the varying of q. As shown in the figure, q = 0.398 are set for S1 to achieve an optimal control performances. This figure also tells that for S1 control, the tip acceleration response of the main span can be well controlled; however, a good control performance for the tip acceleration at the side span cannot be achieved by adjusting the weight parameter. Fig. 5 shows the controlled and uncontrolled tip acceleration response of the side span and the main span when q is set to be 0.398. This figure also tells that the well designed controller can greatly reduce the acceleration response of the tip end of the main span but cannot mitigate the vibration of the side span.

For S2 control, the control system with two AMD carts, whose actuation force expressions are shown as Eq. (10) and (11), installed on the tip ends of both spans of the bridge, is simulated. Numerical studies are conducted when the weighting parameter q varies from 0.01 to 100. Fig. 6 shows the relative RMS ratio of the controlled acceleration response to the uncontrolled acceleration response at the tip end of both spans with the varying of q. As shown in the figure, when q = 9.1, the control system provides the most optimal control performances. This figure also tells that for S2 control, the tip acceleration response of both the main span and the side span can be well reduced. Fig. 7 shows the controlled and uncontrolled tip acceleration time response of the side span and the main span when q is set to be 9.1. This figure also tells that the well designed controller can greatly reduce the acceleration response at the tip end of both spans.
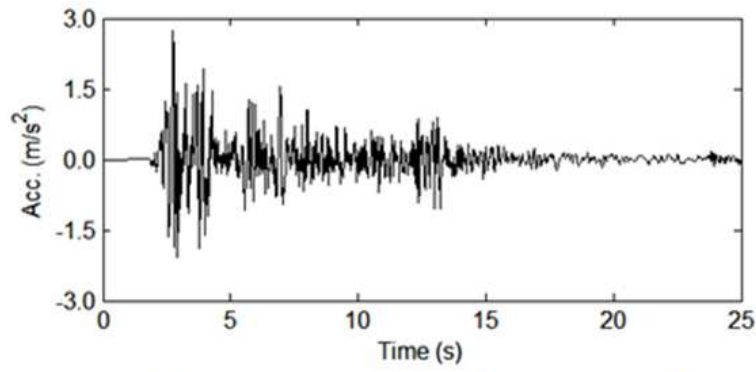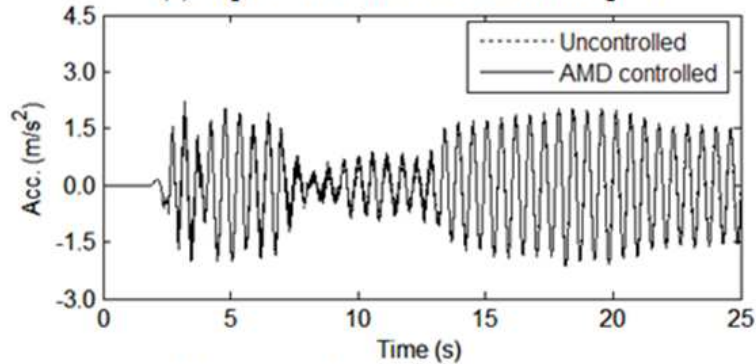
(a) *El Centro* seismic acceleration record

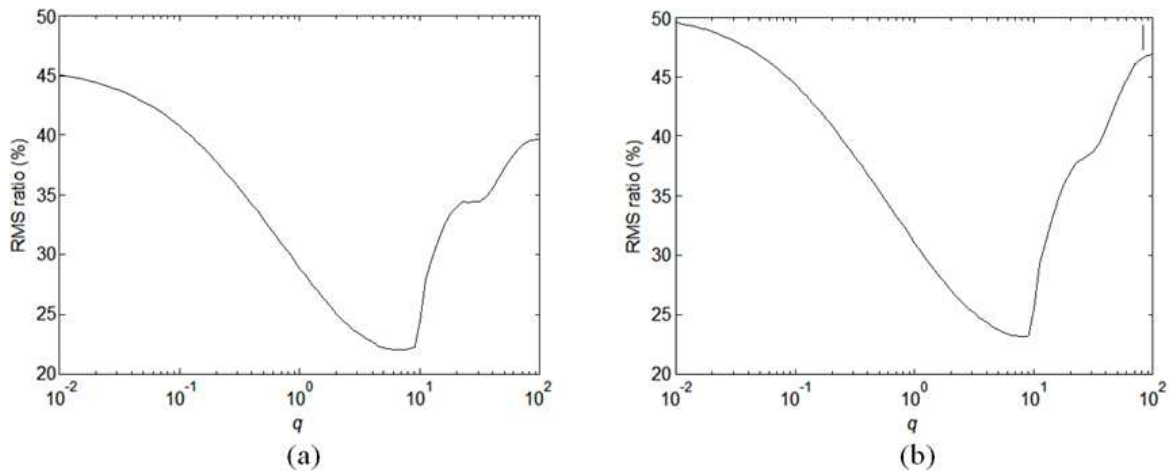(b) Driving voltage of the AMD cart on the tip of the main span
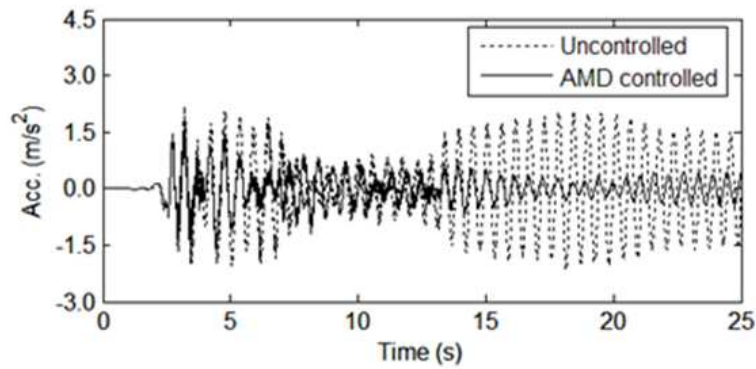
(c) Tip acceleration of the main span

(d) Tip acceleration of the side span

Figure 5. Excitation (a), driving voltage (b), main span tip acceleration (c), and side span tip acceleration (d) time histories of the bridge under El Centro seismic excitation for S1 control

Figure 6. The ratio of the controlled acceleration RMS value to uncontrolled RMS value at the tip ends of the side span (a) and main span (b) with respect to the weighting parameter q for S2 control

The control performance comparison of these two AMD placing strategies tell that for the cable-stayed bridge studied, which is of two dominant transverse vibration modes with close frequencies, the single AMD control strategy (S1) can only reduce structural vibration response of the AMD-instrumented span, and the double AMD control strategy (S2) can achieve a good control performance for reducing structural response of both spans. These observations are verified by checking the controllability criteria. If the control system is of two close eigenvalues, at least two actuators are required to ensure the system is controllable. Moreover, since structural dominant transverse modes are anti-symmetric and symmetric bending modes, the shift of the AMD position along one span of the bridge will only proportionally vary the coefficients of B_r. If two AMDs are placed at one span of the bridge, the corresponding two columns of B_r are linear dependant. Therefore, the two AMDs must be placed at both the side span and the main span respectively to ensure the controllability of the bridge.

6. Experimental implementation

To verify the feasibility of the AMD control for transverse vibration reduction of cable-stayed bridge under construction, an experimental study on the fabricated test model is conducted in the Bridge Testing Laboratory of Tongji University. During the experiment, the S2 control strategy was adopted according to the conclusion obtained from the above numerical simulation study. Fig. 8 shows the layout of the experimental setup. As shown in the figure, the control system includes a data acquisition system, a central control computer, and two AMD carts. The data acquisition system consists of eight accelerometers, whose sensitivity is checked using dynamic calibration method; Dspace signal amplifier and filter; a general purpose data acquisition and control board MultiQ-3, which has 8 single ended analog inputs, 8 analog outputs, 16 bits of digital input, 16 bits of digital output, 3 programmable timers and up to 8 encoder inputs decoded in quadrature (option 2E to 8E). The central control computer is of 512 Mb memory and 1.0 GHz Intel Celeron processor. The
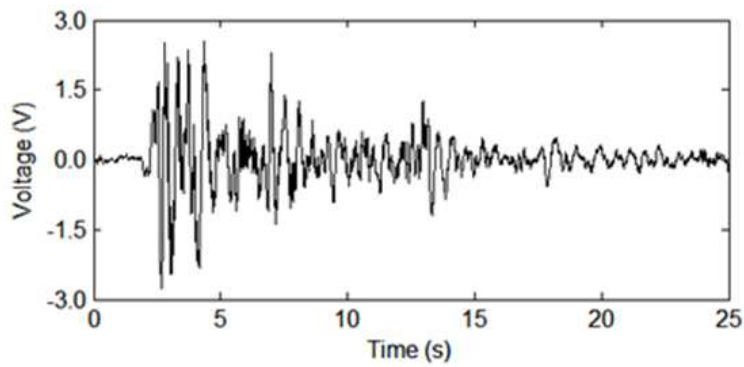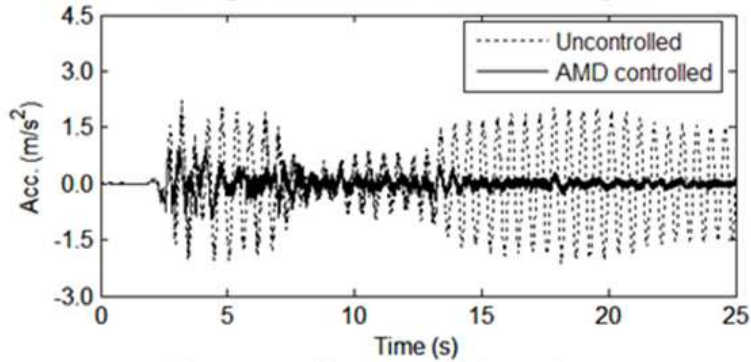
(a) Driving voltage of the AMD cart on the tip of the main span
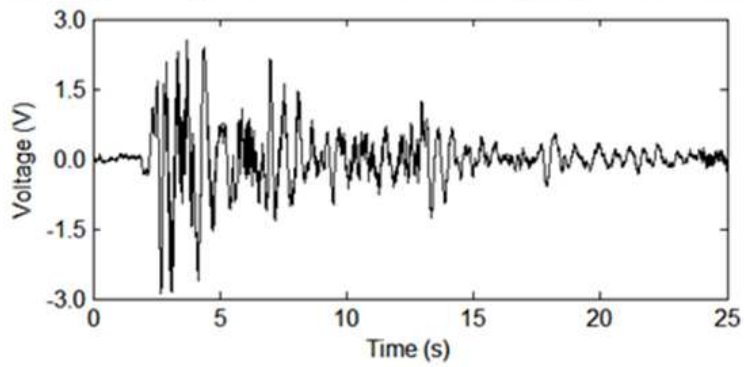
(b) Driving voltage of the AMD cart on the tip of the side span
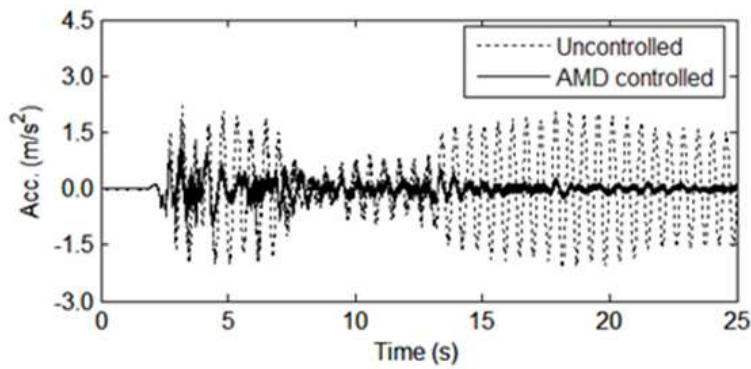
(c) Tip acceleration of the main span

(d) Tip acceleration of the side span

Figure 7. Driving voltage of the main span (a) and side span (b), and tip acceleration time histories of main span (c) and side span (d) of the bridge under *El Centro* seismic excitation for S2 control

AMD carts (as shown in Fig. 8) are electric servo type [16]. They are 0.645 kg weight. Their track length is 32 cm and the max safe input voltage is $\pm 5V$. The system is designed under the constraint of avoiding the AMD to knock the baffle. If the AMD position exceeds the safe range of the orbit, the system will be shut down.
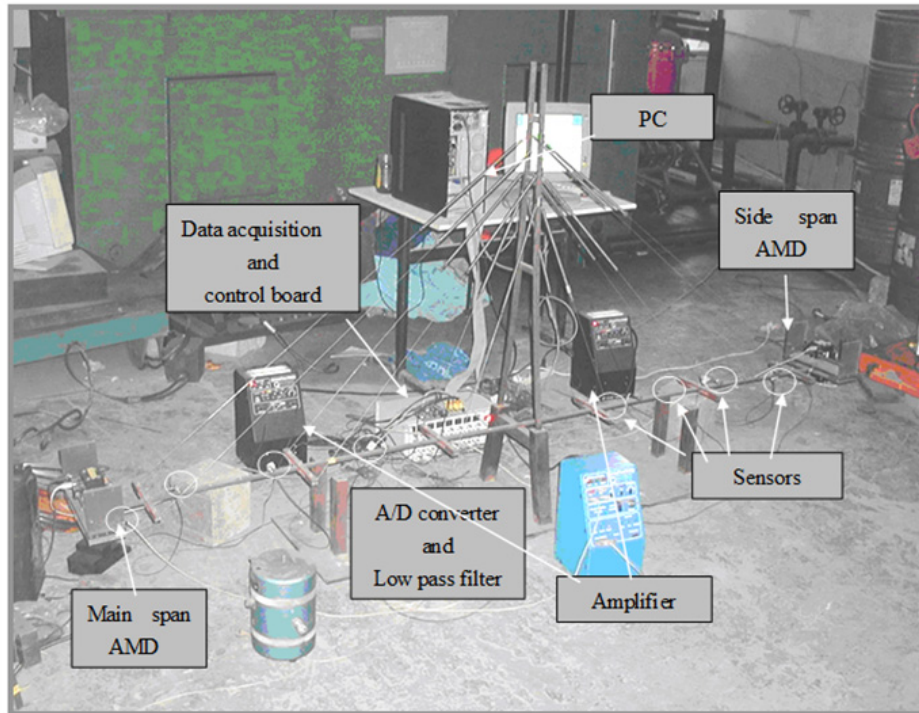
(a)
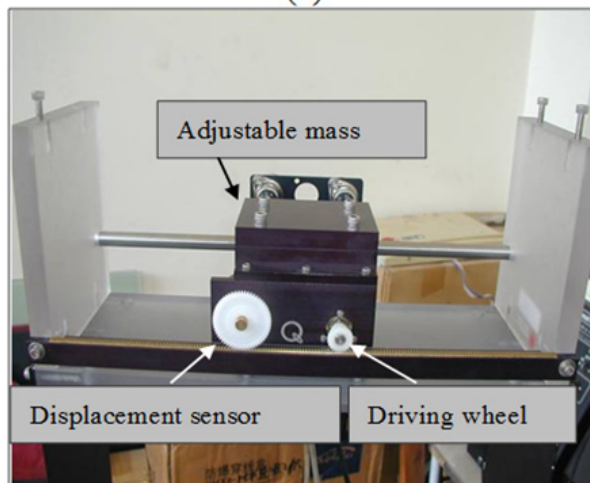
(b)

Figure 8. The experimental setup (a) and the AMD devices (b)

During the experiment, the tip ends of the main girder were pulled transversely using steel wires firstly to generate an initial displacement in this direction. The wires were then cut suddenly and the bridge started to vibrate due to this initial potential energy imported. Several seconds later, the power of the AMD control system was turned on and structural vibration response was recorded. Three case studies were conducted to check the
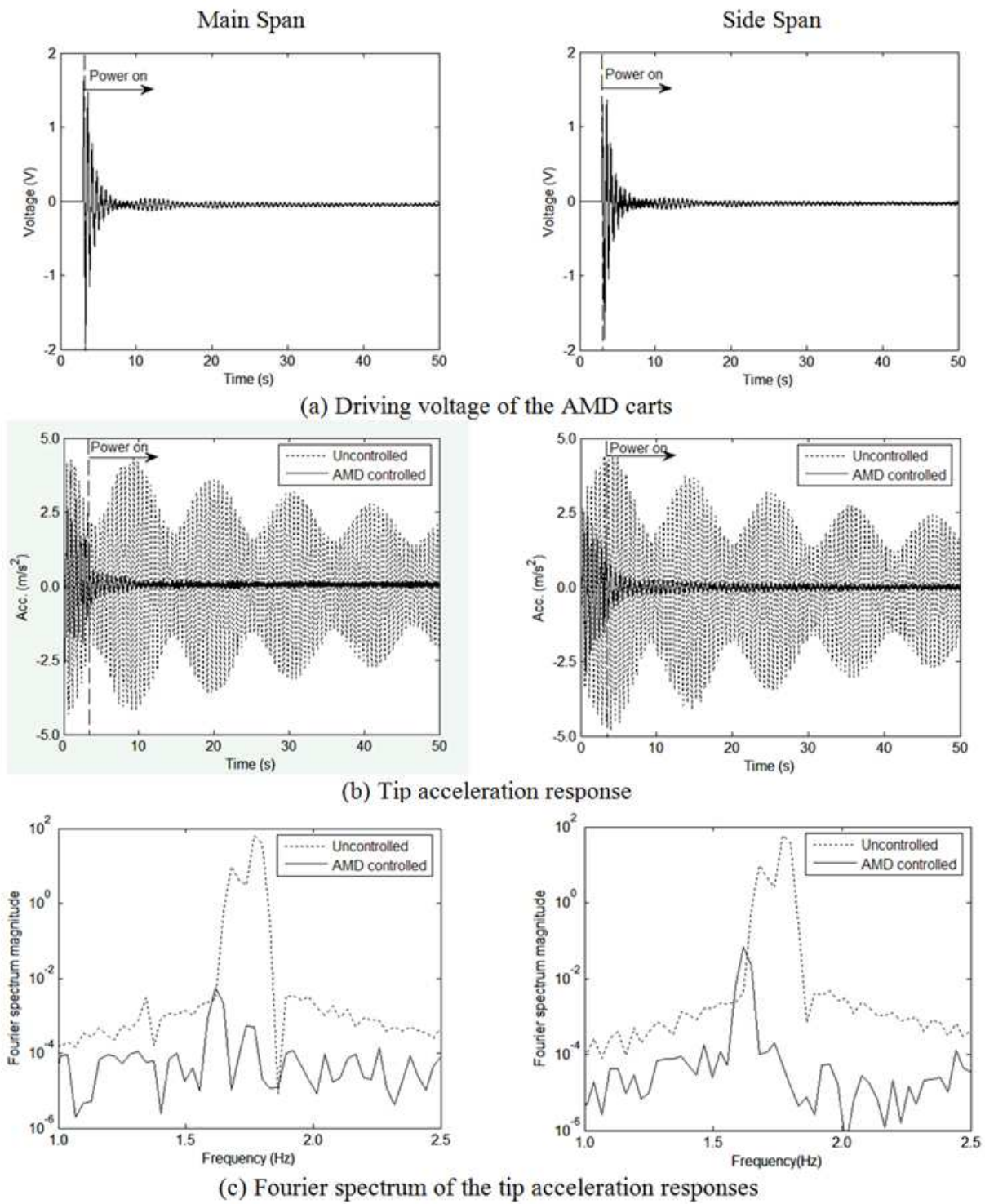
performance of the AMD control system under different excitation schemes. For the first case, case C1, the tip ends of both the main span and the side span were pulled in the same direction. After the steel wires were cut, the transverse symmetric bending mode of the bridge was excited. For case C2, the tip ends of the two spans were pulled in the opposite direction to excite the transverse anti-symmetric bending mode of the bridge. Case C3 simulated bridge free vibration under an initial displacement of the main span. Both anti-symmetric and symmetric transverse bending modes of the bridge would thus be excited.

For test case C1, Fig. 9 shows the AMD driving voltage, recorded tip acceleration responses with or without AMDs, and their Fourier spectrums. As shown in these figures, when the power of the AMD carts was still turned off, structural acceleration responses were already reduced. When the power is turned on, the free decay ratios of structural responses were further increased. That verifies the performance of the active control system on structural response reduction. The comparison of the uncontrolled and AMD controlled Fourier spectrum magnitude of structural responses also verifies this statement. Moreover, as shown, when the AMD carts were installed, the peaks of Fourier spectrum were shifted to the left-hand-side, which meant that the natural frequencies of the system were decreased. Table 5 shows the peak and RMS acceleration response of the structure with and without AMD. As shown in the table, after the AMD was mounted, the peak and RMS accelerations recorded at the tip point of the side span were reduced 44.1 % and 82.1 %, respectively. For the tip point of the main span, the recorded peak and RMS accelerations were reduced 31.1 % and 81.4 %, respectively. For test cases C2 and C3, the peak and RMS acceleration responses of the structure with and without AMD were recorded. As shown in Table 5, the transverse vibration responses for these sensor-mounted points were also efficiently reduced: For case C2, structural peak and RMS acceleration responses were respectively reduced 28.3% and 65.4% for the tip point of the side span and 22.0% and 68.4% for the tip point of the main span; For case C3, structural peak and RMS acceleration responses were reduced 65.8% and 85.6% respectively for the tip point of the side span and 40.5% and 76.7% for the tip point of the main span. Moreover, concerning that the controller is designed via numerical studies on a reduced order model, the good control performances obtained on the bridge model tells that the control algorithm adopted in this study is of good robustness.

Case	Peak acc. of sensor 1		RMS acc. of sensor 1		Peak acc. of sensor 8		RMS acc. of sensor 8	
	No AMD	With AMD	No AMD	With AMD	No AMD	With AMD	No AMD	With AMD
C1	4.431	2.479	1.826	0.326	4.312	2.970	1.810	0.336
C2	4.198	3.012	1.341	0.464	3.563	2.779	1.327	0.419
C3	5.186	1.773	1.800	0.260	5.833	3.473	1.820	0.424

Table 5. Peak and RMS acceleration at the tip ends of the bridge with and without AMDs for the experimental cases

(a) Driving voltage of the AMD carts

(b) Tip acceleration response

(c) Fourier spectrum of the tip acceleration responses

Figure 9. The driving voltage (a) and tip acceleration (b) time histories and Fourier spectrum (c) of responses for control case C1

7. Concluding remarks

In this chapter, the active mass dampers are implemented for vibration control of a lab-scale cable stayed bridge in double cantilever construction state. The results of both numerical

simulation and experimental study verified that the proposed AMD control technique is applicable and efficient for the control of transverse vibration of cable-stayed bridge under construction.

For the cable-stayed bridge studied in this chapter, structural vibration test showed that the bridge was of two dominant transverse bending modes with close frequencies. The numerical study verified that for the control of such a structure with repeated frequencies; at least two AMDs should be installed for a good control performance. Moreover, the placement of those two AMDs should be carefully studied.

For the control of a linear, time-invariant system, an accurate and complete system models are generally required. However, for the bridge-AMD system studied in this chapter, it is very difficult, if not impossible, to set up such a numerical model due to the complex layout of the bridge structure. Since structural vibration responses are generally governed by some dominant vibration modes and the objective of structural vibration control is to reduce but not to completely restrain structural vibration responses, this study verified that a reduced order model constructed from the critical modes is good enough for the controller design to achieve an excellent vibration reduction performance. Considering the differences between the numerical model and the real structure, the control algorithm adopted in this study must be robust to the vibration property change of the controlled structure. The results of experimental studies show that the vibration of the test model can be well controlled using the controller designed from the numerical studies. That means the *LQG* control algorithm is of good robustness for real application.

This study is an initial work on AMD control of transverse vibration of a cable stayed bridge under construction before it can be used for real applications. Although the experimental study verified the efficiency of the adopted AMD control for structural response reduction under given excitation, some primary issues for real application of the AMD control technique, such as how to deal with time delay, how to reduce the requirement on power supply of the control system, and et al., are not addressed in this study. Further laboratory studies or field applications on some real bridges will be conducted in the coming future to discuss these issues and make the technique more efficient and practical for real applications.

Author details

Hao Chen
Institute of Engineering Mechanics, China Earthquake Administration, Sanhe, Hebei, China

Zhi Sun and Limin Sun
State Key Laboratory for Disaster Reduction in Civil Engineering, Tongji University, Shanghai, China

Acknowledgement

8. References

[1] Boonyapinyo, V., Aksorn, A., and Lukkunaprasit, P. (2007). Suppression of aerodynamic response of suspension bridges during erection and after completion by using tuned mass dampers. *Wind and Structures, An Int\'l Journal*, 10(1): 1-22.

[2] Ubertini, F. (2010). Prevention of suspension bridge flutter using multiple tuned mass dampers. *Wind and Structures, An Int\'l Journal*, 13(3): 235-256.

[3] Warnitchai, P., Fujino, Y., Pacheco, B.M. and Agret, R. (1993). An experimental study on active tendon control of cable-stayed bridges. *Earthquake Engineering and Structural Dynamics*, 22: 93-111.

[4] Achkire, Y. and Preumont, A. (1996). Active tendon control of cable-stayed bridges. *Earthquake Engineering and Structural Dynamics*, 25(6): 585-597.

[5] Dyke, S.J., Caicedo, J.M., Turan, G., Bergman, L.A., Hague, S. (2003). Phase I benchmark control problem for seismic response of cable-stayed bridges. *Journal of Structural Engineering, ASCE*, 129(7): 857–872.

[6] Caicedo, J.M., Dyke, S.J., Moon, S.J., Bergman, L.A., Turan, G., Hague, S. (2003). Phase II benchmark control problem for seismic response of cable-stayed bridges. *Journal of Structural Control*, 10: 137–168.

[7] Frederic, B. and Andre, P. (2001). Active tendon control of cable-stayed bridges: a large-scale demonstration. *Earthquake Engineering & Structural Dynamics*, 30: 961–979.

[8] Shelley, S.J., Lee, K.L., Aksel, T. and Aktan, A.E. (1995). Active control and forced vibration studies on highway bridges. *Journal of Structural Engineering, ASCE*, 121(9): 1306-1312.

[9] Korlin, R. and Starossek, U. (2007). Wind tunnel test of an active mass damper for bridge decks. *Journal of Wind Engineering and Industrial Aerodynamics*, 95: 267-277.

[10] Chen, H. (2007). Experimental study on active control of cable-stayed bridge under construction. Master Thesis. Tongji University.

[11] Sun, Z., Hou, W., Chang, C. C. (2009). Structural system identification under random excitation based on asymptotic wavelet analysis. *Engineering Mechanics*, 26(6), 199-204 (in Chinese).

[12] Schemmann, A.G. (1997). Modeling and active control of cable-stayed bridges subject to multiple-support excitation. PhD thesis. Standford University.

[13] Xu, Y. and Chen, J. (2008). Modal-based model reduction and vibration control for uncertain piezoelectric flexible structures. *Structural Engineering and Mechanics*, 29(5): 489-504.

[14] Laub, A.J. and Arnold, W.F. (1984). Controllability and observability criteria for multivariable linear second-order models, *IEEE Transactions on Automatic Control*, AC-29(2).

[15] Wu, J.C., Yang, J.N., and Schmitendorf W.E. (1998). Reduced-order H∞ and *LQR* control for wind-excited tall buildings. *Engineering Structures*. 20(3): 222-236.

[16] Quanser Consulting Inc. (2002). Active Mass Damper: Two-Floor (AMD-2), User Manual.